



**HAL**  
open science

## Echo speckle imaging of dynamic processes in soft materials

Shu Zhang, Jörn Peuser, Chi Zhang, Frédéric Cardinaux, Pavel Zakharov, Sergey E. Skipetrov, Roberto Cerbino, Frank Scheffold

► **To cite this version:**

Shu Zhang, Jörn Peuser, Chi Zhang, Frédéric Cardinaux, Pavel Zakharov, et al.. Echo speckle imaging of dynamic processes in soft materials. *Optics Express*, 2022, 30 (17), pp.30991. 10.1364/OE.459708 . hal-03833992

**HAL Id: hal-03833992**

**<https://hal.science/hal-03833992>**





Submitted on 28 Oct 2022

**HAL** is a multi-disciplinary open access archive for the deposit and dissemination of scientific research documents, whether they are published or not. The documents may come from teaching and research institutions in France or abroad, or from public or private research centers.

L'archive ouverte pluridisciplinaire **HAL**, est destinée au dépôt et à la diffusion de documents scientifiques de niveau recherche, publiés ou non, émanant des établissements d'enseignement et de recherche français ou étrangers, des laboratoires publics ou privés.



# Echo speckle imaging of dynamic processes in soft materials

SHU ZHANG,<sup>1,4</sup>  JÖRN PEUSER,<sup>1,4</sup>  CHI ZHANG,<sup>1</sup> FRÉDÉRIC CARDINAUX,<sup>1</sup> PAVEL ZAKHAROV,<sup>1</sup> SERGEY E. SKIPETROV,<sup>2</sup>  ROBERTO CERBINO,<sup>3</sup>  AND FRANK SCHEFFOLD<sup>1,\*</sup> 

<sup>1</sup>Department of Physics, University of Fribourg, CH-1700 Fribourg, Switzerland

<sup>2</sup>Université Grenoble Alpes, CNRS, LPMMC, 38000 Grenoble, France

<sup>3</sup>Faculty of Physics, University of Vienna, Vienna 1090, Austria

<sup>4</sup>These authors contributed equally

\*frank.scheffold@unifr.ch

<https://www.unifr.ch/phys/en/research/groups/scheffold/>

**Abstract:** We present a laser-speckle imaging technique, termed Echo speckle imaging (ESI), that quantifies the local dynamics in biological tissue and soft materials with a noise level around or below 10% of the measured signal without affecting the spatial resolution. We achieve this through an unconventional speckle beam illumination that creates changing, statistically independent illumination conditions and substantially increases the measurement accuracy. Control experiments for dynamically homogeneous and heterogeneous soft materials and tissue phantoms illustrate the performance of the method. We show that this approach enables us to precision-monitor purely dynamic heterogeneities in turbid soft media with a lateral resolution of 100  $\mu\text{m}$  and better.

© 2022 Optica Publishing Group under the terms of the [Optica Open Access Publishing Agreement](#)

## 1. Introduction

Dynamic speckle imaging methods have been used in biomedical imaging since the early 1980s and were initially based on laser speckle contrast analysis (LASCA) using photographic film [1–4]. LASCA and related methods obtain spatially resolved information about blood flow by dividing the original speckle image into small regions of interest (ROI), each part counting typically tens of statistically independent speckles. In each ROI, the contrast of the speckle pattern is measured for a fixed exposure time of the film or camera detector. ROIs, where the blood velocity is higher due to capillary perfusion flow, show a lower contrast of the corresponding speckle pattern. Calculation of the speckle contrast in each ROI provides a coarse-grained dynamic version of the original image, consisting of fewer meta-pixels.

Over the last two decades, we have seen the advent of a wealth of new laser-speckle based experimental techniques to monitor tissue blood flow but also dynamics in non-living soft materials, for instance, gels, foams, emulsions, pastes, and hard-sphere glasses [5–7]. Recent advances in optical sensor technology make most of these novel approaches possible. A modern digital CCD (charge-coupled device) or CMOS (complementary metal-oxide-semiconductor) sensor contains millions of detectors, which allow massive parallel registration of many intensity values of independent speckle spots. Early applications in far-field speckle detection are for example ‘multi-speckle dynamic light scattering’ [8,9], ‘time-resolved correlation spectroscopy’ (TRC) [10] or ‘speckle visibility spectroscopy (SVS) [7,11]. While these investigations in the 1990s and early 2000s have been performed in the far-field of the scattering sample, later experiments, starting around 2010, investigated the near-field regime [6,12–16], where speckle imaging is capable of providing space-resolved maps of the dynamical activity of soft materials. Speckles imaged close to the scattering sample are referred to as *near-field speckles* [5,6,17] in contrast to the more conventional far-field speckles. However, in general, near field speckles have

little connection with the so-called optical near field of evanescent waves probed, for example, with scanning near field optical microscopy [18]. Recent experiments also introduce more refined approaches in that they measure the degree of correlation between the speckle fields at different times utilizing the intensity correlation function [12,19,20], or the intensity structure-function [15,21].

One severe limitation that emerged very clearly from well-controlled studies is grounded in the non-ergodic and non-stationary nature of soft materials and blood flow dynamics in tissue. Moreover, the speckle contrast, correlation (or structure) function has to be determined experimentally with the required accuracy on a time scale shorter than the time over which the system changes, for biomedical applications about one second. Taking temporal averages is usually insufficient since they differ from proper (ergodic) spatial averages. The problem could be overcome by using an active speckle-noise reduction scheme described in [23], which is, however, too slow and inefficient for most applications.

To obtain data with acceptable noise, one thus calculates ensemble averages by collecting many speckle spots (i.e., different camera pixels) in a large ROI. The trade-off between time resolution and accuracy typically leads to low-resolution images that are still significantly affected by statistical noise [21,24–26]. Let us give an example. In order to reduce the noise (standard deviation)/signal of the correlation coefficient  $\sigma_c(t, \tau)/c(t, \tau)$  to better than 10% one needs to sample approximately  $N \approx 1000$  statistically independent speckle intensity values or sample more than  $30 \times 30$  camera pixels, if the speckle size is matched to the pixel size of typically  $10 \mu\text{m}$ , as it is usually done [21]. Therefore, the nominal resolution is reduced from  $10 \mu\text{m}$  to  $300 \mu\text{m}$  for a magnification of one. For a VGA sensor ( $640 \times 480$  pixels) the meta-image contains less than  $20 \times 20$  meta-pixels, which is prohibitive. In practice, smaller regions of interest are usually defined, typically  $5 \times 5$  or  $7 \times 7$  pixels leading to noisy images [2].

In this article, we present a rapid acquisition laser-speckle imaging technique that quantifies the dynamics of soft materials with accurate statistical estimators without affecting the spatial resolution. We achieve this through an unconventional speckle beam illumination that creates rapidly changing, statistically independent illumination conditions combined with periodic cycling and synchronized image acquisition [22]. Our echo speckle imaging (ESI) technique provides the time correlation or structure coefficient and thus corresponds to 'dynamic light scattering imaging' (DLSI) [19], a powerful variant of laser speckle imaging. Unlike LASCA, the latter directly links the measured signal to dynamics and scattering properties in the sample.

## 2. Principle and experimental setup

In our experiments, a digital camera records the surface intensity pattern  $I(x, y)$  of light reflected from an optically dense scattering medium [27,28]. The experimental setup is presented in Fig. 1. The camera (Prosilica GC 655, pixel size  $a = 9.9 \mu\text{m}$ ) records images with  $0.81\times$  magnification and its aperture set to produce image speckle roughly of the order of the size of a camera pixel. We calculate the spatial intensity correlation function of the speckle pattern and find a speckle size of 1.2 pixels, for details see Ref. [21]. A collimated laser beam (Coherent Verdi V5,  $\lambda = 532 \text{ nm}$ ) is slightly focused and directed to a ground glass using a microscope objective. The size  $w_0$  of the illumination spot can be adjusted by positioning the objective relative to the ground glass. The forward-scattered light is collimated using a lens with a focal length  $f = 7.5 \text{ cm}$ , thus creating a homogeneous speckle beam with a width of  $2.5 \text{ cm}$  set by the diameter of the lens. The illumination speckles should be comparable in size or smaller than the transport mean free path  $l^*$  of the sample under study. This ensures that a proper ensemble average is obtained by having many statistically independent scattered field amplitudes to interfere locally [29]. We obtain this condition by creating longitudinally elongated near-field speckles and using them to illuminate the sample placed at about  $10 \text{ cm}$  from the lens. In this *deep-Fresnel* regime, the speckles have a

Gaussian shape with a constant size  $b \approx \pi\lambda f/w_0$  [30,31], which in our case amounts to about 50–100 microns, see also [29].

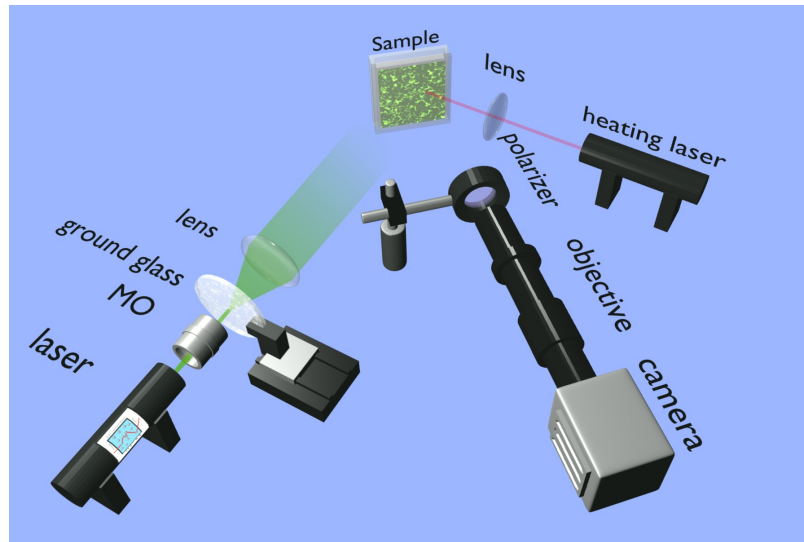


**Fig. 1.** Experimental setup : A focused laser beam is positioned on a ground glass using a 10× microscope objective (MO). The emerging speckle beam is collimated by a lens ( $f = 75$  mm). The ground glass is mounted on a precision motorized stage that oscillates with an amplitude of 1 mm at a selected frequency of 0.2–1 Hz. The collimated speckle beam is used to illuminate the sample. A CCD camera with an objective is used to image the sample surface. A crossed polarizer is mounted on the objective to select a well-defined polarization state and to suppress specular reflections. A heating laser can be employed to locally melt thermosensitive structures such as gelatin gels and thus create well-defined dynamic heterogeneities. Moving the ground glass creates different realizations of the speckle beam, which allows one to obtain local statistical averages without the need for extensive spatial averaging.

The speckle beam is obtained in such a way that it impinges on the sample, and the scattered light is recorded in the image plane. The reason for employing a speckle incident beam is that we can now apply a displacement of the ground glass with a precision translation stage (Fig. 1). Compared to earlier speckle echo experiments using a spinning ground glass diffuser [15,22], the translation stage allows us to reduce the velocity of the ground glass diffuser (no speckle blurring during acquisition) while still creating sufficiently many statistically independent speckle beams. In our previous speckle imaging work, Ref. [15] due to the fast motion of the ground glass, speckle images were significantly blurred and the experimental values of  $d_2(t, \tau)$  substantially reduced.

A key feature of our work is that we synchronize the movement of the translation stage and the data acquisition by using the electronic output of the translation stage as a trigger for the camera. This ensures that the image pair we are correlating is captured at the same position on the stage for each cycle of duration  $t_{\text{echo}}$ . There is no periodic stop for the image acquisition time and the ESI-acquisition time is  $2t_{\text{Echo}}$ . Apart from the fact that we need to scan the ground glass twice (to compare all speckle image pairs), we do not need any time averaging.

The translation stage used is a voice-coil actuated stage (V-106.11S, Physik Instrumente GmbH, Germany) with a digital encoder. The positional accuracy (reproducibility) is 0.2 micron, and the stage is operated with a periodicity of  $t_{\text{Echo}} \sim 1\text{--}5$  s with a 1 mm amplitude. The average speed of motion is thus  $v = 2 \text{ mm}/t_{\text{Echo}}$ . The typical stage-displacement required to de-correlate the speckle beam for our settings is  $x_c \approx 3.3 \mu\text{m}$  which corresponds to a decorrelation time of

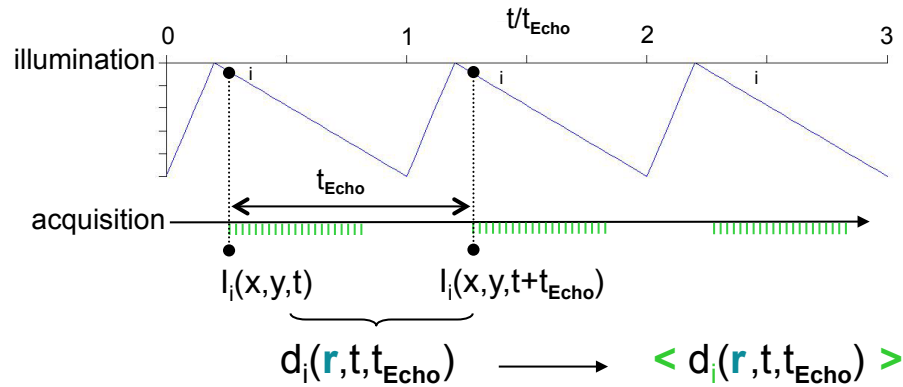


**Fig. 2.** Principle of Echo Speckle Imaging (ESI): A series of typically 100 statistically independent speckle images is recorded at a given frame rate  $1/\tau_0 \sim 50$  fps (frames per second). After one cycle of duration  $t_{\text{Echo}}$  the procedure is repeated. The intensity structure coefficient  $d_i(r, t, t_{\text{Echo}})$  is computed using all equivalent pairs of images spaced by a lag time  $t_{\text{Echo}}$ . The procedure can be repeated at time lags  $\tau = n \times t_{\text{Echo}}$  with  $n = 2, 3, 4, \dots$ . The statistical accuracy can be further improved by limited spatial averaging over  $2 \times 2$  or  $3 \times 3$  pixels.

$\tau_c = x_c/v \sim 1.7\text{--}8.3$  ms. The exposure time of the camera  $T_{\text{exposure}} \sim 0.1\text{--}1$  ms is set much shorter, while the time difference between individual images  $\tau_0 = 20$  ms is much longer. In contrast to earlier work, Ref. [15], our scheme prevents the blurring of individual images due to the motion of the stage while ensuring that subsequently recorded speckles are statistically independent (Fig. 2). To synchronize the movement of the translation stage and the data acquisition, we use the electronic output of the translation stage as a trigger signal for the camera, operating at typically 50 fps. This ensures that the images are captured at the same stage position for each cycle. Note that we create more than 1000 uncorrelated speckle beams during a single oscillation cycle. Due to the limited frame rate of the digital camera used (50 fps at  $640 \times 480$ ), as well as memory and software limitations, we only use a fraction of those (i.e. 100) for the statistical analysis. However, one could easily overcome this limitation using faster hardware, allowing for an additional order of magnitude increase in statistical accuracy or improved time resolution.

### 3. Noise in echo speckle imaging

We expect our echo speckle acquisition, to be equivalent when sampling the properties of an image speckle in space or, for a fluctuating speckle in time [21]. To demonstrate this equivalence, we perform two different experiments. First, we carry out a time correlation experiment on a slowly relaxing sample. We disperse about 3.3 wt% of polystyrene microspheres (diameter 710 nm) in an aqueous solution of cetylpyridinium chloride/sodium salicylate (100 mM CPyCl/60 mM NaSal). The resulting surfactant solution strongly scatters light with a transport mean free path  $l^* \approx 73 \mu\text{m}$  for a vacuum wavelength  $\lambda = 532$  nm. Reference [32] gives a detailed characterization of the system. The surfactant solution displays strongly viscoelastic properties with a slow terminal relaxation. We keep the sample at room temperature during our measurement, which sets the relaxation time to several tens of seconds. Illuminating the sample with an expanded collimated laser beam, we calculate the (full frame) multi-speckle temporal intensity correlation function (ICF)

$$g_2(t, \tau) = \langle I(t - \tau/2) I(t + \tau/2) \rangle / \langle I \rangle^2 \quad (1)$$

or equivalently the correlation coefficient  $c(t, \tau) = g_2(t, \tau) - 1$ . The brackets indicate averages taken over statistically independent speckle, in time or in space. For standard multi-speckle experiments the correlation (delay) time  $\tau$  is a multiple of the reciprocal frame rate, 1/50 sec, for Echo-measurements a multiple of  $t_{\text{Echo}} = 1 - 5$  sec. For stationary sample dynamics,  $c(t, \tau) = g_2(t, \tau) - 1$  becomes independent of the time  $t$  when the measurement is performed.

Dividing the image in areas of size  $N$  also allows us to determine, as a function of  $N$ , the noise of the speckle correlation coefficient, which is given by the normalized variance of the correlation coefficient

$$\frac{\sigma_c(t, \tau)^2}{\langle c(t, \tau) \rangle^2} = \frac{\langle c(t, \tau)^2 \rangle - \langle c(t, \tau) \rangle^2}{\langle c(t, \tau) \rangle^2} \quad (2)$$

with  $\sigma_c(t, 0)^2 / \langle c(t, 0) \rangle^2 \approx 8/N$  as shown in Ref. [21]. The noise of the correlation coefficient increases with increasing  $\tau$ , for details see [21]. We repeat the same procedure with the speckle beam illumination in place by choosing a fixed periodicity of  $t_{\text{Echo}} = 1.45$  s. As shown in Fig. 3, for a full frame analysis, both approaches lead to identical results for the normalized temporal autocorrelation function. In Fig. 3 we show that taking statistical averages in space or time, analyzing echoes, or a mix of both, leads to the same results. Our results demonstrate that we can replace spatial averaging on the CCD matrix with echo time-averaging. We repeat the procedure for light reflected from a solid piece of Teflon (thickness  $\approx 1$  cm) with a typical photon transport mean free path  $l^* \approx 0.25$  mm.

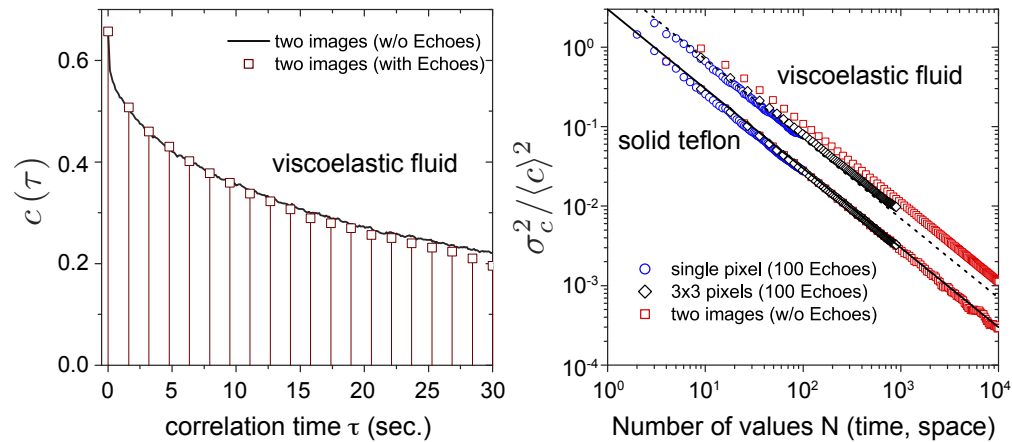


**Fig. 3.** Left: Intensity correlation coefficient measured for a viscoelastic fluid with a slow terminal relaxation time (100 mM CPyCl/60 mM NaSal and 3.3% of polystyrene microspheres, diameter 710 nm, in water.  $l^* \approx 73 \mu\text{m}$ ,  $t_{\text{Echo}} = 1.45$  s). We plot the results of conventional multi-speckle correlation spectroscopy [8,9,22] analyzing pairs of full speckle images without echoes (translation stage at rest,  $N \approx 3 \cdot 10^5$ ). Solid symbols: Echo speckle analysis of full images. Both give the same results at  $t_{\text{Echo}}$  and multiples. We note that  $c(\tau = 0) < 1$  due to the finite millisecond exposure time. Right: Normalized variance of the correlation coefficient in echo-speckle imaging of the viscoelastic fluid for  $\tau = t_{\text{Echo}} = 1.45$  s compared to the conventional multi-speckle approach. Averaging on the CCD matrix in time or space gives the same statistical accuracy. Data for solid Teflon is also shown with  $l^* \approx 0.25$  mm,  $t_{\text{Echo}} = 5.4$  s. Solid and dashed lines are power-law fits  $\propto 1/N$  [21].

The results obtained for the variance, Eq. (2) are in agreement with an earlier study of statistical noise in laser speckle imaging techniques, predicted to scale as  $1/N$  [21]. The noise of the structure coefficient  $d_2(t, \tau) = \langle [I(t - \tau/2) - I(t + \tau/2)]^2 \rangle / \langle I \rangle^2$  is comparable to the one of the correlation coefficient at short times, with  $\sigma_{d_2}^2 / \langle d_2 \rangle^2 \approx 5/N$ , and does not depend on the

correlation time  $\tau$  [21]. It is worth recalling here that in the limit of perfect measurement statistics, the correlation and the structure coefficients are related by  $d_2(t, \tau) = 2 [c(t, 0) - c(t, \tau)]$ , and that the structure-function is known to outperform the correlation function concerning accuracy when the collection time is limited. Further, it is less sensitive to low-frequency noise or drifts [33]. From this analysis, we find that we can measure the correlation and structure coefficient with an accuracy better than 10% (standard deviation divided by mean) by averaging over  $3 \times 3$  pixels in space and 100 pixels in time using echoes ( $N = 900$ ).

#### 4. Imaging dynamic heterogeneity

Our goal is to image an optically homogeneous sample with dynamic heterogeneities. To demonstrate the performance of ESI for high-resolution dynamic imaging, we have designed several model experiments. Our sample is a homogeneous mixture of about 4 wt% of  $\text{TiO}_2$  powder dispersed in a 4 wt% aqueous gelatin solution. Based on previous studies using the same material [34,35] we estimate  $l^* \approx 15 \mu\text{m}$  at  $\lambda = 532 \text{ nm}$ . We note that in our experiment,  $l^*$  is smaller than the speckle size. Consequently, we observe a residual spatial variance in the intensity pattern post-averaging. Details about this effect are discussed elsewhere [29]. While the intensity structure coefficient is little affected, the residual intensity variations can influence the intensity correlation coefficient (not shown). We could overcome this problem with a modified optical design and choose a smaller speckle size, but it is more convenient to work with the structure coefficient instead. The latter is also a more direct measure of dynamic activity, which is the appropriate quantity we wish to study. We add a sufficient amount of a commercial green food dye to the gelatin sample with a strong absorption band for the red light. Subsequently, we fill the gelatin sample in a glass cuvette (Hellma) with typical dimensions  $10 \times 5 \times 25 \text{ mm}^3$  and let it rest at room temperature for at least 12 h. Due to the high gelatin concentration, the sample solidifies, and the speckle pattern becomes stationary. With a tightly focused red HeNe laser beam ( $\lambda = 633 \text{ nm}$ ), steered using two Galvano mirrors, we locally melt the gelatin by dissipating heat generated by absorption of light. The actual size of the melted volume is not limited by the focus of the laser beam (below  $20 \mu\text{m}$ ) but by a complicated interplay between light absorption, heat diffusion, and the melting transition of gelatin. In practice, we can create in the sample dynamic heterogeneities below  $100 \mu\text{m}$ . We again use a green ( $\lambda = 532 \text{ nm}$ ) speckle beam and probe the dynamic heterogeneities outside the absorption band.

Figures 4(a) and (b) show two typical examples of such an experiment where we calculate the structure coefficient. The image on the left in Fig. 4(a) shows the result of heating at a fixed point using the standard imaging approach (no echos), while the same situation is analyzed on the right using ESI. Due to the significantly better signal-to-noise ratio, only the ESI image provides a quantitative map of the sample dynamics. While the previous example is stationary in time, we also want to test ESI in a situation where the sample properties evolve. Figure 4(b) shows snapshots of a movie where the melting beam is moved continuously over the sample. The full movie is available as a supplementary material. The images illustrate that using ESI; we can indeed monitor such a dynamic process in real-time on time scales equal or longer than the echo period  $t_{\text{Echo}} \gtrsim 1 \text{ sec}$ . Using more advanced hardware, we could further reduce the temporal resolution towards the subsecond range. Such an implementation of ESI would require a more intense laser and fast digital camera. For more rapid data acquisition and synchronization with the camera, we could also replace the translation stage and ground glass with a digital-micromirror device (DMD) [36].

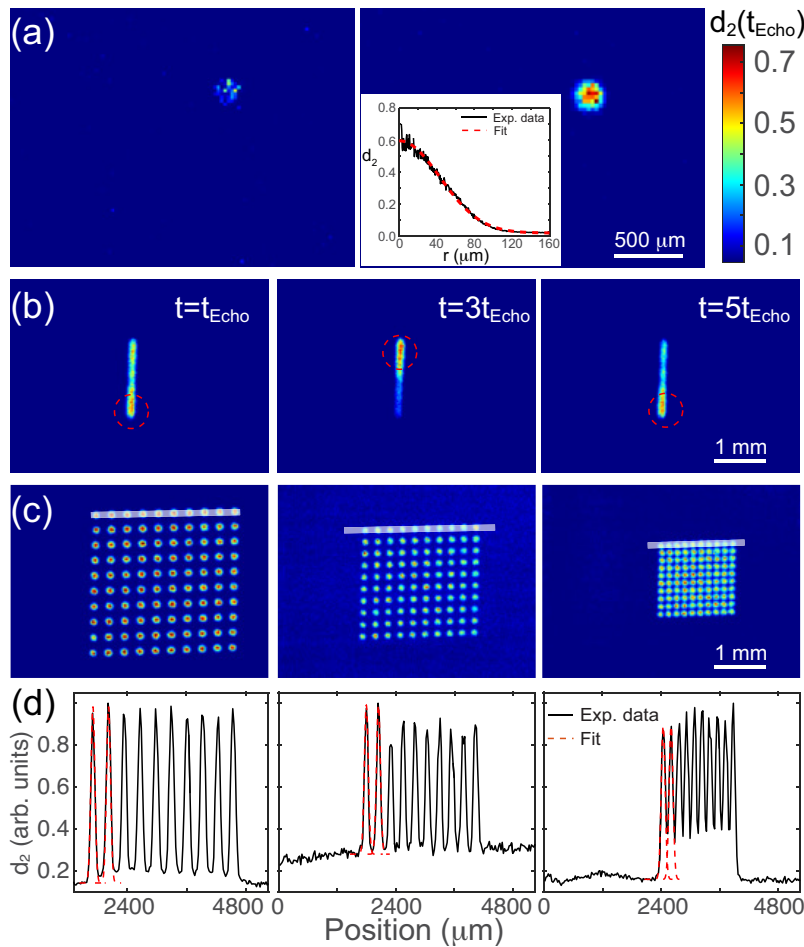


**Fig. 4.** (a) Map of dynamical activity during local melting of a sample by selective heating with a focused laser beam. The sample consists of 4 wt% of  $\text{TiO}_2$  powder dispersed in a 4 wt% aqueous solution of gelatin with green food dye added ( $l^* \approx 15 \mu\text{m}$ ,  $t_{\text{Echo}} = 5.4 \text{ s}$ ). Spatially resolved structure-function obtained from left: simple spatial speckle statistics ( $3 \times 3$  pixels for each meta pixel,  $N = 9$ ) and right: averaging over 100 echoes and  $3 \times 3$  pixels ( $N = 900$ ). Although the spatial resolution is the same, the ESI pictures substantially improve S/N (signal to noise ratio). The inset shows the image profile for the ESI image along the radial direction from the center of the melting point, which is fitted by a Gaussian function. The fitting parameter of the standard deviation  $\sigma$  is  $43 \mu\text{m}$ . (b) Map of dynamical activity of the gelatin sample was obtained through time-resolved echo imaging. Snapshots are taken while the melting (red) laser beam is moved over the sample (see Visualization 1). (c) Map of dynamical activity of the gelatin sample for an array of points written by melting the gelatin sample locally. Spatially resolved structure-function is obtained by averaging over 100 echoes and  $3 \times 3$  pixels ( $N = 900$ ),  $t_{\text{Echo}} = 5.4 \text{ s}$ . The spacing between the points is varied from  $314 \mu\text{m}$  to  $150 \mu\text{m}$ . (d) The image profiles for the ESI images along the indicated white lines are shown in (c). The red dash line is the Gaussian fit for all experiments with the same  $\sigma \sim 43 \mu\text{m}$ .



## 5. Spatial resolution

The spatial resolution in ESI is an important parameter. The image magnification and the  $3 \times 3$  pixels spatial averaging window means that a single square meta-pixel has an edge length of  $24 \mu\text{m}$ . However, the image speckles are formed by multiply scattered light diffusely reflected from a superficial layer. About half of the photons exit the sample at a transverse distance  $r_{x,y} \leq 2.7l^*$  from the entrance point [3,12]. Due to the diffuse scattering, the length scale probed in the  $z$  direction (i.e., perpendicular to the sample surface) is of the same order. Thus, at any given point on the sample surface, the speckle fluctuations are determined by the dynamics in a scattering volume of size roughly  $(3l^*)^3$ . Whenever  $3l^*$  is equal to or larger than the meta pixel edge length, the sample's effective spatial resolution is set by the transport mean free path and not by the imaging optics or data processing. For the experimental conditions described in section 4,  $3l^* \sim 45 \mu\text{m}$  is slightly larger than a meta pixel, and thus we should be able to resolve dynamic heterogeneities on length scales on the order of  $50 \mu\text{m}$ .

### 5.1. Melting points and arrays

Experimentally, we assess the spatial resolution by analyzing the signal of individual melting spots or by creating a variety of melting points, rapidly scanning the positions of a  $10 \times 10$  points array. The spacing between the points is reduced from  $314 \mu\text{m}$  to  $150 \mu\text{m}$ . Even in the latter case, individual points can be identified, Fig. 4(c) and (d). We find that in both cases, the nominal resolution is about  $90 \mu\text{m}$ , demonstrating that an actual spatial resolution in an imaging experiment can be at or below the  $100 \mu\text{m}$ -range using ESI. We also show snapshots of a movie (supplemental material), Fig. 4(b), where the laser knife is moved continuously over the sample.

### 5.2. Phantom imaging measurements

We perform additional speckle imaging measurements by embedding a capillary filled with a liquid colloidal suspension in the same solid gelatin/TiO<sub>2</sub> matrix described above. The liquid sample consists of a ten wt% polystyrene latex beads with a diameter of  $195 \text{ nm}$  ( $l^* \sim 20 \mu\text{m}$ ). The thin rectangle capillary (inner dimensions  $0.01 \times 0.1 \text{ mm}$ ) is immersed in the gelatin sample and is flush with the cuvette wall, see inset Fig. 5(a). The optical properties of the suspension and the matrix are similar, and the capillary and matrix show little optical contrast. This medical phantom mimics blood flow in a liquid capillary inclusion in solid tissue. The laser speckle imaging maps for different measurement configurations are shown in Fig. 5. For all cases, we define a target statistical accuracy by fixing the number of statistically independent intensity values to  $N = 900$ , corresponding to statistical noise to signal  $\sigma_d(t, \tau)/d(t, \tau) \sim 7\%$ . We have to collect  $30 \times 30$  intensity values or pixels with only spatial averaging. With a meta-pixel edge length of  $240 \mu\text{m}$ , we cannot resolve the capillary. By adding more and more information using the echo signal, from panel (b)-(d), we improve the spatial resolution until we reach a plateau with a meta pixel size of  $24 \mu\text{m}$ , smaller than  $3l^*$  of both the latex suspensions and the gelatin/TiO<sub>2</sub> matrix. Further reduction of the meta pixel size would lead to oversampling since the resolution is limited by the scattering process or  $l^*$  and not the measurement or data acquisition. In parallel to adding the echo-signal, we sacrifice time resolution from  $\tau_0 = 20 \text{ ms}$  to  $t_{\text{Echo}} \sim 5 \text{ sec}$ . Our phantom measurement is not optimized for the shortest acquisition time, and it would be straightforward to reach  $N = 900$  on sub-second timescales, required to monitor e.g. cerebral hemodynamics [28], using a faster camera. In the inset of Fig. 5(d), we show an ESI-cross section perpendicular to the capillary's orientation and averaged along a small segment of the long axis. We fit the line with a top hat function of width  $100 \mu\text{m}$  convoluted with a Gaussian and find smearing of  $2\sigma = 90 \mu\text{m}$ , in agreement with the results shown in Fig. 4.

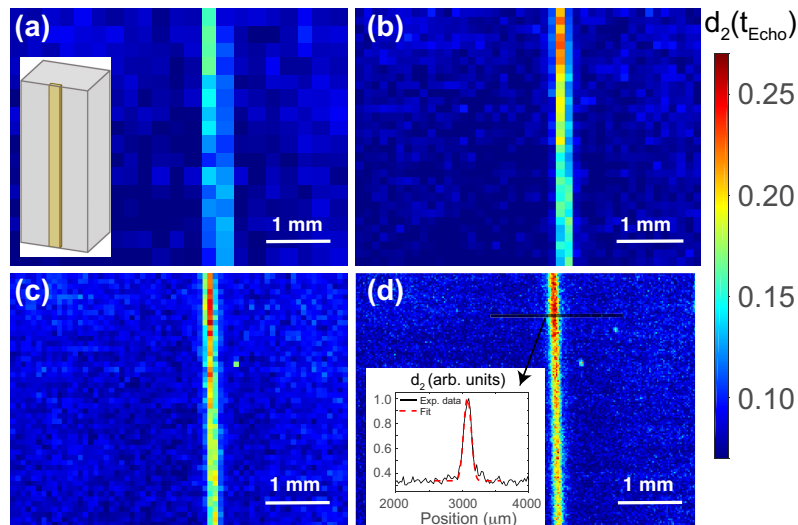


**Fig. 5.** Map of dynamical activity of Brownian motion of polystyrene particles (10% solids suspension in water with a diameter of 195 nm) filled in a thin rectangle capillary (inner diameters  $0.01 \times 0.1$  mm) which is immersed in the gelatin sample as shown in (a) inset. The sample consists of 4 wt% of  $\text{TiO}_2$  powder dispersed in a 4 wt% aqueous gelatin solution. The optical properties for the gelatin and colloidal suspension match ( $l^* < 50 \mu\text{m}$ ) and create dynamic contrast. (a)-(d): Spatially resolved structure-function obtained from averaging over 1 echo and  $30 \times 30$  pixels, 4 echoes and  $15 \times 15$  pixels, 9 echoes and  $10 \times 10$  pixels, and 100 echoes and  $3 \times 3$  pixels ( $N = 900$ ), respectively.  $t_{\text{Echo}} = 5.4$  s. The inset of (d) shows a signal profile along the grey line in the main panel. The red dashed line in the inset is a convolution of a top-hat function (width  $100 \mu\text{m}$ ) with a Gaussian with  $\sigma = 45 \mu\text{m}$  for the best fit to the experimental data.

## 6. Summary and conclusions

In summary, we have shown that using speckle beam illumination with a ground glass diffuser and by analyzing correlation echoes, we can reduce noise in laser speckle imaging by at least one order of magnitude. We achieve the latter without speckle blurring due to the diffuser's motion. In contrast to previous speckle imaging experiments on soft materials [12,16], the actual resolution of ESI is set exclusively by the optical transport mean path of a turbid sample. Consequently, there is no need to perform extensive spatial averages anymore to achieve sufficient statistical accuracy. Moreover, ESI provides the time correlation or structure coefficient and thus corresponds to 'dynamic light scattering imaging'. Our low-noise speckle imaging method can be considered a quantitative tool to characterize blood flow in tissue, thermal dynamics, or deformations in soft glassy materials or gels. It offers substantial benefits for biomedical imaging applications without adversely affecting the time resolution. Our results open the door for many possible applications to study slow, spatially heterogeneous relaxations in complex fluids such as dense emulsions, dispersions, slurries, pastes, or granular media.

**Funding.** Schweizerischer Nationalfonds zur Förderung der Wissenschaftlichen Forschung (182881, 183651, 188494).

**Acknowledgments.** The Swiss National Science Foundation financially supported this work through the National Center of Competence in Research Bio-Inspired Materials, No. 182881, and projects No. 188494, No. 183651. We thank Bruno Weber and Matthias Wyss for discussions and in-vivo test experiments performed in their laboratory.

**Disclosures.** F.S. is a board member and shareholder of LS Instruments AG, Fribourg, Switzerland.

**Data availability.** Data underlying the results presented in this paper are not publicly available at this time but may be obtained from the authors upon reasonable request.

## References

1. J. D. Briers and S. Webster, "Laser speckle contrast analysis (lasca): a non-scanning, full-field technique for monitoring capillary blood flow," *J. Biomed. Opt.* **1**(2), 174–179 (1996).
2. A. K. Dunn, H. Bolays, M. A. Moskowitz, and D. A. Boas, "Dynamic imaging of cerebral blood flow using laser speckle," *J. Cereb. Blood Flow Metab.* **21**(3), 195–201 (2001).
3. P. Zakharov, A. Völker, M. Wyss, F. Haiss, N. Calcinaghi, C. Zunzunegui, A. Buck, F. Scheffold, and B. Weber, "Dynamic laser speckle imaging of cerebral blood flow," *Opt. Express* **17**(16), 13904–13917 (2009).
4. M. Draijer, E. Hondebrink, T. van Leeuwen, and W. Steenbergen, "Review of laser speckle contrast techniques for visualizing tissue perfusion," *Lasers Med. Sci.* **24**(4), 639–651 (2009).
5. F. Scheffold and R. Cerbino, "New trends in light scattering," *Curr. Opin. Colloid Interface Sci.* **12**(1), 50–57 (2007).
6. F. Giavazzi and R. Cerbino, "Digital fourier microscopy for soft matter dynamics," *J. Opt.* **16**(8), 083001 (2014).
7. D. Bossert, J. Natterodt, D. A. Urban, C. Weder, A. Petri-Fink, and S. Balog, "Speckle-visibility spectroscopy of depolarized dynamic light scattering," *J. Phys. Chem. B* **121**(33), 7999–8007 (2017).
8. S. Kirsch, V. Frenz, W. Schärtl, E. Bartsch, and H. Sillescu, "Multispeckle autocorrelation spectroscopy and its application to the investigation of ultraslow dynamical processes," *J. Chem. Phys.* **104**(4), 1758–1761 (1996).
9. V. Viasnoff, F. Lequeux, and D. Pine, "Multispeckle diffusing-wave spectroscopy: A tool to study slow relaxation and time-dependent dynamics," *Rev. Sci. Instrum.* **73**(6), 2336–2344 (2002).
10. L. Cipelletti, H. Bissig, V. Trappe, P. Ballesta, and S. Mazoyer, "Time-resolved correlation: a new tool for studying temporally heterogeneous dynamics," *J. Phys.: Condens. Matter* **15**(1), S257–S262 (2003).
11. R. Bandyopadhyay, A. Gittings, S. Suh, P. Dixon, and D. J. Durian, "Speckle-visibility spectroscopy: A tool to study time-varying dynamics," *Rev. Sci. Instrum.* **76**(9), 093110 (2005).
12. M. Erpelding, A. Amon, and J. Crassous, "Diffusive wave spectroscopy applied to the spatially resolved deformation of a solid," *Phys. Rev. E* **78**(4), 046104 (2008).
13. A. Amon, A. Mikhailovskaya, and J. Crassous, "Spatially resolved measurements of micro-deformations in granular materials using diffusing wave spectroscopy," *Rev. Sci. Instrum.* **88**(5), 051804 (2017).
14. H. M. van der Kooij and J. Sprakel, "Watching paint dry; more exciting than it seems," *Soft Matter* **11**(32), 6353–6359 (2015).
15. P. Zakharov and F. Scheffold, "Monitoring spatially heterogeneous dynamics in a drying colloidal thin film," *Soft Mater.* **8**(2), 102–113 (2010).
16. A. Duri, D. A. Sessoms, V. Trappe, and L. Cipelletti, "Resolving long-range spatial correlations in jammed colloidal systems using photon correlation imaging," *Phys. Rev. Lett.* **102**(8), 085702 (2009).
17. R. Cerbino and A. Vailati, "Near-field scattering techniques: Novel instrumentation and results from time and spatially resolved investigations of soft matter systems," *Curr. Opin. Colloid Interface Sci.* **14**(6), 416–425 (2009).
18. H. Heinzelmann and D. Pohl, "Scanning near-field optical microscopy," *Appl. Phys. A* **59**(2), 89–101 (1994).
19. D. D. Postnov, J. Tang, S. E. Erdener, K. Kılıç, and D. A. Boas, "Dynamic light scattering imaging," *Sci. Adv.* **6**(45), eabc4628 (2020).
20. T. Durduran and A. G. Yodh, "Diffuse correlation spectroscopy for non-invasive, micro-vascular cerebral blood flow measurement," *NeuroImage* **85**, 51–63 (2014).
21. S. E. Skipetrov, J. Peuser, R. Cerbino, P. Zakharov, B. Weber, and F. Scheffold, "Noise in laser speckle correlation and imaging techniques," *Opt. Express* **18**(14), 14519–14534 (2010).
22. P. Zakharov and D. Scheffold, "Multispeckle diffusing-wave spectroscopy with a single-mode detection scheme," *Phys. Rev. E* **73**(1), 011413 (2006).
23. A. C. Völker, P. Zakharov, B. Weber, F. Buck, and F. Scheffold, "Laser speckle imaging with an active noise reduction scheme," *Opt. Express* **13**(24), 9782–9787 (2005).
24. P. Zakharov, A. Völker, A. Buck, B. Weber, and F. Scheffold, "Quantitative modeling of laser speckle imaging," *Opt. Lett.* **31**(23), 3465–3467 (2006).
25. J. W. Goodman, *Speckle phenomena in optics: theory and applications* (Roberts and Company Publishers, 2007).
26. D. D. Duncan, S. J. Kirkpatrick, and R. K. Wang, "Statistics of local speckle contrast," *J. Opt. Soc. Am. A* **25**(1), 9–15 (2008).
27. A. Yodh and B. Chance, "Spectroscopy and imaging with diffusing light," *Phys. Today* **48**(3), 34–40 (1995).
28. P. Zakharov, F. Scheffold, and B. Weber, "Laser speckle imaging of cerebral blood flow," in *Optical Imaging of Neocortical Dynamics*, (Springer, 2014), pp. 255–271.
29. F. Scheffold and I. D. Block, "Rapid high resolution imaging of diffusive properties in turbid media," *Opt. Express* **20**(1), 192–200 (2012).
30. R. Cerbino, "Correlations of light in the deep fresnel region: An extended van cittert and zernike theorem," *Phys. Rev. A* **75**(5), 053815 (2007).
31. D. Magatti, A. Gatti, and F. Ferri, "Three-dimensional coherence of light speckles: experiment," *Phys. Rev. A* **79**(5), 053831 (2009).
32. P. Fischer and H. Rehage, "Rheological master curves of viscoelastic surfactant solutions by varying the solvent viscosity and temperature," *Langmuir* **13**(26), 7012–7020 (1997).

33. K. Schätzel, "Noise in photon correlation and photon structure functions," *Opt. Acta: Internat. J. Opt.* **30**(2), 155–166 (1983).
34. P. Balog, "Scattering and propagation of light in mesoscopic random media," Ph.D. thesis, University of Fribourg, Switzerland (2007).
35. S. Balog, P. Zakharov, F. Scheffold, and S. Skipetrov, "Photocount statistics in mesoscopic optics," *Phys. Rev. Lett.* **97**(10), 103901 (2006).
36. G. Gauthier, I. Lenton, N. M. Parry, M. Baker, M. Davis, H. Rubinsztein-Dunlop, and T. Neely, "Direct imaging of a digital-micromirror device for configurable microscopic optical potentials," *Optica* **3**(10), 1136–1143 (2016).